Available online at www.sciencedirect.com
SCIENCE DIRECT®
Journal of Sound and Vibration 270 (2004) 951–980
JOURNAL OF SOUND AND VIBRATION
www.elsevier.com/locate/jsvi

Hull vibration excitation due to monopole and dipole propeller sources

R. Kinns[a,*], C.D. Bloor[b]

[a] RKAcoustics, Glenavon, Back Road, Clynder, Dunbartonshire G84 0QQ, UK
[b] Department of Applied Mathematics and Theoretical Physics, University of Cambridge, Silver Street, Cambridge CB3 9EW, UK

Received 6 June 2001; accepted 6 February 2003

Abstract

An acoustic boundary element (BE) model of a modern twin-screw cruise liner is used to show how fluctuating pressures above the propeller, and hull forces that cause ship vibration, change relative to each other with the nature of propeller sources. The effects of fluctuating loads on the propeller, represented by dipole sources in different directions, are compared with the effects of monopole sources at one and two times maximum propeller blade passing frequency. Convergence of results for the cruise liner model is demonstrated using different element distributions. The results are specimen transfer functions that relate propeller sources, having general spectral characteristics, to hull excitation. They are presented in non-dimensional form to facilitate comparison with results for other hull shapes and to demonstrate the effect of hull scale.

A simple analysis of dipole and monopole sources is used to interpret results and to demonstrate why solution of the Helmholtz equation, which includes the effects of a finite speed of sound underwater, is needed for accurate evaluation of hull disturbing forces. It is argued that such modelling techniques can facilitate more accurate future interpretation of model-scale experimental data from towing tanks or water tunnels, as well as allowing improved specification of ship acoustic requirements.

1. Introduction

Considerable effort has been devoted to the prediction of fluctuating pressures in the vicinity of cavitating and non-cavitating propellers. The emphasis on hull pressure arose originally from the desire to avoid risk of fatigue damage to hull plating, but it is common to find that the maximum

*Corresponding author. Tel.: +44-0-1436-831245; fax: +44-0-1436-831031.
E-mail address: rogerkinns@aol.com (R. Kinns).

0022-460X/$ - see front matter © 2003 Elsevier Ltd. All rights reserved.
doi:10.1016/S0022-460X(03)00641-2

hull pressures in modern twin-screw ships are far below levels where fatigue damage is likely. Now, the focus is on ensuring that induced vibration will not cause passenger discomfort. The accuracy of predictions of hull pressure fluctuations near the propeller is being improved continually by refinement in model-scale experiments [1] and numerical techniques. Many of the available methods are summarized by Breslin and Andersen [2]. Recent developments include increasingly comprehensive descriptions of propeller sources and the effects of boundary constraints [3]. Careful interpretation of fluctuating pressure is, however, needed to determine the disturbing forces that cause hull vibration.

Various limitations of model-scale experiments have been recognized previously [2], but it has also been usual to assume that water can be treated as an incompressible fluid, having an infinite speed of sound. In effect, the fluctuating pressure anywhere on the hull surface is assumed to respond instantaneously to changes in the disturbing source. The incompressible Bernoulli's equation can be used in numerical simulation of propeller sources [2,4], but there are consequent errors in calculation of pressures away from the immediate vicinity of the propeller, and therefore in total hull forces, that increase with source frequency. In a real ship having a length of 250 m, for example, it would take 0.17 s for sound to travel underwater from one end to the other, if the underwater speed of sound is 1500 m/s. It would take longer still, if the speed of sound is reduced by bubble content. The simple effects of time delays in changing the relative phase of sinusoidal signals are compounded by frequency-dependent diffraction around the hull and the effects of the free surface of the sea.

Retarded time effects are not the same in model-scale and full-scale experiments, because the model-scale wavelength of underwater sound λ is usually too large in relation to hull dimensions at a given scaled frequency. Reproduction of Froude number with a $1/s$ scale model, for example, leads to a factor of $\sqrt{s}$ error in λ at scaled propeller blade passing frequency (*bpf*), if the speed of underwater sound is fixed.

The pressure field which causes hull vibration is distributed over a large area of the hull. Furthermore, the nature of the hull pressure distribution changes substantially with the nature of the propeller sources at a given frequency. It also changes with boundary conditions, so that precise representation of the wake field, propeller and cavitation behaviour in a water tunnel or towing tank is insufficient, however detailed the measurements of fluctuating pressure on the hull above the propeller. Despite these limitations, maximum fluctuating hull pressures at multiples of propeller *bpf* often feature in contracts for ships that have to meet demanding vibration standards, to the exclusion of factors that are equally if not more important. Such a specification can lead to sub-optimal selection of parameters like propeller diameter and tip clearance, because maximum pressure fluctuations change much more rapidly with distance of a given source from the hull than the disturbing forces which govern vibration response.

The aim of this paper is to lay the foundations for more accurate determination of hull vibration excitation due to different types of propeller source. The approach differs from that used previously, in that the propeller is regarded as a set of superimposed acoustic sources, whose influence on hull vibration excitation can be determined by solving the wave equation in the presence of the hull surface and the free surface of the sea. Acoustic boundary element (BE) modelling techniques are used to determine the pressure field on a complex hull shape due to prescribed acoustic sources. The potential of the approach and typical results are demonstrated by representing the shape of a modern twin-screw cruise liner hull. It is assumed throughout that

sources are sufficiently weak and concentrated in position that the fluid outside the source region can be regarded as linear and homogenous, with a constant density and speed of sound.

Determination of the acoustic source distribution requires a detailed analysis of the propeller in a moving fluid, leading to estimation of fluid cavity volume fluctuations associated with cavitation, as well as the rotating and fluctuating forces on the blades and the effects of finite blade thickness. All of these influences can be represented as acoustic sources of different types and complexity, varying with both the propeller design and its operating condition. Such sources can be estimated using a combination of numerical and experimental techniques for hydrodynamic analysis, where the effects of fluid flow are encapsulated in the source derivation. For example, dipole sources are introduced by momentum transfer to the moving fluid from monopole sources that are stationary relative to the hull [2]. The relative importance of different sources, so far as hull vibration excitation is concerned, depends strongly on the nature of the pressure fields that they induce on the hull. For this reason, determination of the pressure field due to a given acoustic source has been separated deliberately from the determination of its strength, which is outside the scope of the present paper. A valuable simplification in ship analysis is that the Mach number is always small, so that the fluid can be regarded as stationary so far as determination of the hull pressure field due to a given acoustic source at the propeller is concerned. Typically, the forward speed of the ship is less than 1% of the speed of sound.

Once significant cavitation has developed on the propeller blades, a simple stationary monopole, located at the position of maximum cavitation volume, represents the dominant source term in many cases of practical interest. Previous emphasis [5,6] has therefore been on sources having acoustic monopole characteristics. Predictions of hull pressure and force distributions show how interference effects are present at frequencies as low as typical values of *bpf*, and are substantial at twice *bpf*, in the case of the representative cruise liner. Such sources will not, however, necessarily govern the hull pressure distribution near the propeller.

The fluctuating pressures on the hull surface due to dipole sources can have larger magnitudes than those due to monopole sources, while leading to much weaker hull excitation. Recent results for twin-screw fast ferries [7], where hull forces are estimated by integration of pressure over a small area of hull surface on the same side as the propeller, have shown how non-cavitating sources can dominate local pressure at high power, while causing lower disturbing forces than cavitating sources on even this limited region of the hull. The fluid is assumed to be incompressible in Ref. [7], but the complete range of propeller sources, including the influence of the rotating pressure field due to blade thickness, is included. It will be demonstrated how the relative influence of cavitation sources can be amplified further when integration is over a larger proportion of the hull surface.

In this paper, the emphasis is on the effects of fluctuating propeller blade forces, which can be represented as stationary dipole sources at the hub, relative to the effects of a stationary monopole. The consequent disturbing forces on a surface ship hull are found to be a significant proportion of those applied to the hub and propeller shaft. Presentation in non-dimensional form allows the comparative effects of monopole and dipole sources to be examined easily for a given wavelength relative to hull dimensions. Subsequent development will include representation of rotating steady forces and finite blade thickness as acoustic sources of appropriate order.

Results from the acoustic BE model of a cruise liner hull show how care is needed in the interpretation of both model-scale and full-scale hull pressure measurements. They also suggest

how corrections might be introduced to give improved predictions of hull excitation from model tests with dissimilar boundary conditions to the full-scale environment.

2. Application of the Helmholtz equation

The propagation of sound waves through a static fluid medium is governed by the wave equation

$$\nabla^2\phi - (1/c^2)\partial^2\phi/\partial t^2 = 0, \tag{1}$$

where ϕ is the velocity potential, depending on position and time, and c is the speed of sound. This can be established by consideration of the equation of continuity and conservation of momentum [8]. It reduces to Laplace's equation if c is infinite. In deriving this equation, it is assumed that the disturbances to the fluid are small and hence terms of second order or higher in amplitude can be ignored. It has also been assumed that the fluid is infinite. The effect of surfaces in the fluid is to introduce source terms in the right hand side of Eq. (1).

It is convenient to investigate the problem in the frequency domain, because the assumption of linearity means that any arbitrary disturbance can be represented as a sum of sinusoidal components. Substitution for ϕ in Eq. (1) with $\phi = \Phi e^{i\omega t}$, where ω is the angular frequency, leads to the Helmholtz equation

$$\nabla^2\Phi + k^2\Phi = 0, \tag{2}$$

where $k = \omega/c$ is the wave number.

The surface integral equation formulation of the Helmholtz equation, developed by Kirchhoff [9], can be derived directly by an application of the Green theorem [10]. Application of the Green theorem for the pressure perturbation p leads to the (Kirchhoff–) Helmholtz equation

$$p(\mathbf{r}) = \int_S [e^{-ik|\mathbf{r}-\mathbf{r}'|}/\{4\pi|\mathbf{r}-\mathbf{r}'|\}]\partial p(\mathbf{r}')/\partial n \, dS - \int_S p(\mathbf{r}')\partial/\partial n(e^{-ik|\mathbf{r}-\mathbf{r}'|}/\{4\pi|\mathbf{r}-\mathbf{r}'|\}) \, dS, \tag{3}$$

where $\mathbf{r}$ is the location of pressure measurement in the fluid and $\mathbf{r}'$ is a point on the bounding surface S. The first integral expresses the monopole field due to the surface velocity distribution, while the second can be interpreted as the dipole field of the surface pressure.

3. Solution using boundary elements

An integral equation can be derived from Eq. (3), by taking the limit as $\mathbf{r}$ approaches a point $\mathbf{r}'$ on the hull surface and applying the boundary conditions. This expresses the known incident pressure field p_{inc} at $\mathbf{r}'$ as an integral over the surface of, for example, the unknown field p times the normal derivative of the Green function.

In order to solve this integral equation, the hull surface is subdivided into, say, n elements or 'patches'. The integral can be rewritten as a sum of n sub-integrals over these elements. Assuming the surface pressure p is constant over each element [11], it can be taken outside the integral,

giving rise to n unknowns, say p_i. The resulting equation can be applied at any $\mathbf{r}'$ on the hull, and in particular at the centre of each of the n surface elements. This therefore gives rise to a set of n linear equations in the n unknowns

$$p_{inc}(r_i) = \sum\nolimits_j (c_{ij} p_j). \tag{4}$$

The constants c_{ij} in Eq. (4) represent terms related to the normal derivative of the Green function. The problem is thereby reduced to that of inverting a matrix equation. In the limit of infinitesimally small elements, that is $n \to \infty$, the solution will be exact. The element distribution can be chosen to match the expected parameter distribution, concentrating elements where changes are likely to be most rapid. Convergence can be checked by varying the number and distribution of elements.

3.1. BE model of a cruise liner hull

A numerical description of a real cruise liner hull was used in Ref. [5] to illustrate application of the modelling techniques to a real hull shape. The same hull description is used here. The hull is typical of modern twin-screw cruise liners having a single skeg.

The hull has a waterline length l of 251 m and a beam b of 32.2 m. The draught w is 8.3 m in level trim. The propeller disc is 8.4 m forward of the stern waterline at this condition. The emphasis in this paper is on results at 12 and 24 Hz. These are the maximum values of one and two times propeller *bpf* in the ship selected for detailed analysis. The underwater sound wavelength λ is, respectively, 125 and 62.5 m, corresponding to $3.88b$ and $1.94b$. It will be shown that there are significant changes with frequency in the nature of hull force distributions due to fluctuating forces at the propeller when wavelength changes in this range.

The effects of non-cavitating sources on vibration are almost always negligible at $2bpf$ or higher multiples of *bpf*, so far as surface ship hull excitation is concerned [2,7]. This includes the effects of blade thickness, which leads to a rotating pressure field on the hull, as well as rotating steady forces and fluctuating forces due to variations in blade loading. It is therefore appropriate to concentrate on results at *bpf*, so far as non-cavitating sources are concerned.

The parameters x, y and z represent longitudinal distance from the stern waterline, transverse distance from the ship centreline and vertical distance from the waterline, respectively. These parameters are positive in the forward, starboard and upward directions.

3.2. Presentation of results in non-dimensional form

The beam b is used as the reference length scale throughout this paper, allowing all the results to be presented in a convenient non-dimensional form. Table 1 shows the principal physical dimensions of the ship and their non-dimensional values. Physical and non-dimensional values of selected sea surface extents in the BE model, sound wavelengths and wave numbers are also included. The non-dimensional forms of source strengths, hull forces and hull pressures are specified in Table 1. For clarity in discussion, results are described as being at *bpf* or a specified low multiple of *bpf*, in order to show dependence on sound wavelength relative to hull beam. The non-dimensional wavelength λ/b is 3.88, 1.94 and 0.97 at *bpf*, $2bpf$ and $4bpf$, respectively. The corresponding non-dimensional wave numbers kb are 1.62, 3.24 and 6.47.

Table 1
Physical and non-dimensional parameters

Parameter	Notation	Dimension	Value	Dimensionless parameter	Dimensionless value
Beam	b	m	32.2	Unity	Unity
Waterline length	l	m	251.0	l/b	7.80
Nominal draught	w	m	8.3	w/b	0.26
Axial propeller location	x_s	m	8.4	p/b	0.26
Surface extent in BE model	e	m	100	e/b	3.11
			200		6.21
			300		9.32
			400		12.42
Blade passing frequency	f at bpf	Hz	12		
	f at $2bpf$		24		
	f at $4bpf$		48		
Wavelength at blade passing frequency	λ at bpf	m	125	λ/b	3.88
	λ at $2bpf$		62.5		1.94
	λ at $4bpf$		31.25		0.97
Wave number at blade passing frequency	k at bpf	m^{-1}	0.050	kb	1.62
	k at $2bpf$		0.101		3.24
	k at $4bpf$		0.201		6.47
Monopole source strength	M_0	kg/s^2 or N/m			
Dipole source strength	D_0	N			
Hull force due to monopole	F_m	N		$F_m/(M_0 b)$	
Hull force due to dipole	F_d	N		F_d/D_0	
Hull pressure due to monopole	p_m	N/m^2		$p_m b/M_0$	
Hull pressure due to dipole	p_d	N/m^2		$p_m b^2/D_0$	

3.3. Representation of the hull and sea surfaces

There are two types of boundary constraint in the numerical model. The first constraint is that fluctuating pressure is zero at the surface of the sea, while the second is that fluctuating velocity is zero normal to the hull surface. Thus, the sea acts as a pressure release surface, while the hull acts as a rigid boundary. The first constraint is appropriate at frequencies of more than a few Hz, for typical propeller dimensions and immersion. It can be shown [2] that fluid inertial effects are much more important than the effects of gravity in the frequency range of interest here.

The effects of hull flexibility can be included in a complete model, but this requires representation of the internal structure as well as surface shape. The effects of vibratory response on the pressure field can be considered separately, the 'blocked' pressure representing the underlying excitation [12]. Indeed, it is usual in model-scale experiments to specify a high-impedance structure, so that model vibration is minimized. The sea surface is assumed to be flat in the present analysis, but surface waves that move with the ship can be included if desired.

The acoustic sources can have arbitrary complexity and motion, but it is shown explicitly in Ref. [2] how a complex, but compact, cavitation region can be modelled as a single stationary monopole source, so far as determination of pressures away from the immediate vicinity of the propeller are concerned. It is the net source strength, rather than the detailed characteristics of the propeller source and local pressure fluctuations, that governs overall hull excitation. The same type of approximation can be used to determine the principal effects of fluctuating forces that are distributed over propeller blades.

The sea surface e in the BE model is defined for a specified extent either side of the hull, as far forward as the bow. The surface extends by the same distance in the stern direction. An extent of 300 m, corresponding to $e/b = 9.32$, has been used for most of the analysis in this paper, as shown in Fig. 1, but it will be demonstrated that almost identical results can be obtained using other extents and element distributions. The basic model uses 600 elements to describe the hull, with an additional 1176 elements to describe the sea surface. The hull elements are distributed between 25 longitudinal segments, with 24 elements around the hull in each segment. This model has sufficient resolution when $\lambda/b > 1.5$, but the number of elements has to be increased when the wavelength is reduced further, in order to ensure that elements are sufficiently small on the scale of λ to ensure convergence.

Fig. 2 shows the surface element distribution on the hull itself, for the starboard side only. The hull, but not the assumed excitation, is symmetric. For clarity, elements are shown for alternate longitudinal stations, specified according to distance x/b from the stern waterline. Larger numbers of elements in either or both of the longitudinal or transverse directions, as well as different sea surface extents, are used to check convergence.

3.4. Representation of propeller sources

The fluctuating forces on the propeller blades can be represented as forces and moments at multiples of *bpf* at the hub, in a simplified analysis. The fluctuating forces and moments applied to

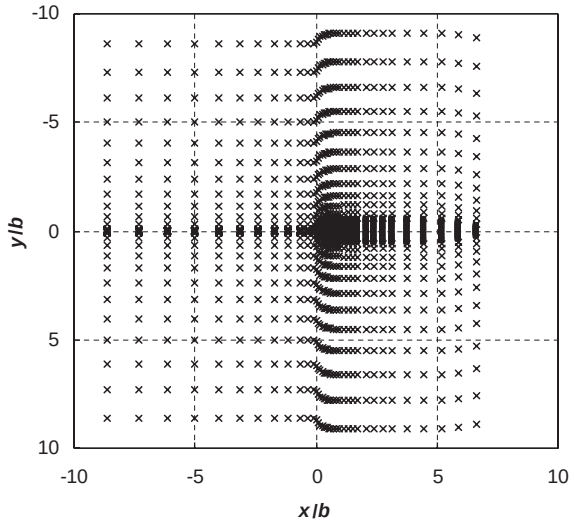

Fig. 1. Boundary element distribution: (×) sea surface; (■) hull surface.

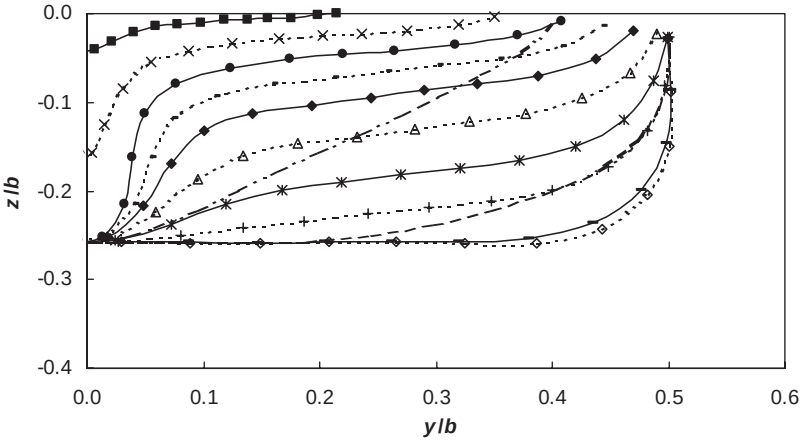

Fig. 2. Boundary element distribution on starboard hull surface. Hull sections shown for $x/b = 0.11$, 0.25, 0.40, 0.54, 0.72, 0.98, 1.34, 1.70, 2.42, 3.12, 4.47 and 5.91.

the propeller shaft, which excite the hull via the shaft bearings, are equal and opposite to those applied to the fluid. The moments are inefficient generators of fluctuating pressure in relation to forces at low frequencies and can be ignored for the present purpose. Thus, the principal effects can be explored by representing the propeller as a set of tri-axial dipoles at its hub, fluctuating sinusoidally at *bpf* and its harmonics.

3.5. Source locations

Fig. 3 shows the selected locations of sources in the plane of the propeller disc. Fig. 3 also shows hull sections near to the propeller disc. Sources are positioned at locations along the vertical and transverse diameters of the propeller. An additional monopole source is shown at 40° inboard on the periphery of the propeller disc, which was found to be close to the position of peak cavitation volume on the propeller blades when they rotate inwards in the wake field [13].

4. Pressure fields due to monopole and dipole sources

The following analysis is derived from [14]. The sound field due to a point monopole is

$$p_m = \mathrm{i}\omega Q_0 \mathrm{e}^{\mathrm{i}(\omega t - kr)}/(4\pi r), \tag{5}$$

where ω is the radian frequency; Q_0 the mass flux amplitude; k the wave number $= 2\pi/\lambda$; r the distance from source to receiver.

The field due to a compact doublet is

$$p_d = \omega^2 Q_0 s\{1 - \mathrm{i}/kr\}\cos\theta \mathrm{e}^{\mathrm{i}(\omega t - kr)}/(4\pi r c_0), \tag{6}$$

where s is the doublet separation $\ll\lambda$; θ the angle between the doublet axis and the receiver; c_0 the speed of sound.

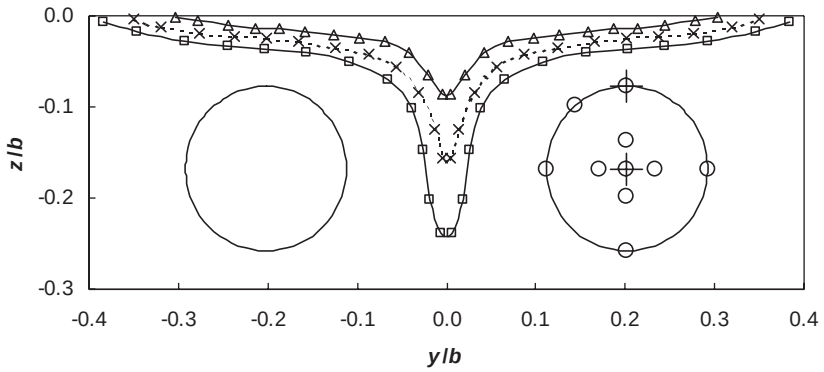

Fig. 3. Source positions relative to hull surface: (—△—) section at $x/b = 0.18$; (- - × - -) section at $x/b = 0.25$; (—□—) section at $x/b = 0.32$; (○) monopole position; (+) dipole position; (———) propeller at $x/b = 0.26$.

The field due to a fluctuating force with amplitude D_0 is

$$p_f = \mathrm{i}\omega D_0\{1 - \mathrm{i}/kr\}\cos\theta \mathrm{e}^{\mathrm{i}(\omega t - kr)}/(4\pi r c_0). \tag{7}$$

The pressure fields due to the force and doublet are the same if

$$D_0 = -\mathrm{i}\omega s Q_0, \tag{8}$$

The maximum rate of change of mass flux M_0 is related to Q_0 by

$$M_0 = \mathrm{i}\omega Q_0, \tag{9}$$

so that

$$D_0 = -sM_0. \tag{10}$$

The far-field pressure amplitude along the axis of the dipole force D_0 is the same as that due to a single monopole with strength M_0 if

$$D_0 = \lambda M_0/(2\pi). \tag{11}$$

The pressure close to a single monopole is in phase with the rate of change of mass flux, while the near field ahead of a doublet is in phase with the pressure due to its positive monopole. The phase of the acoustic field ahead of the doublet is retarded by 90° relative to its positive monopole source.

4.1. Near-field and far-field pressure fluctuations

Figs. 4 and 5 show the essential characteristics of monopole and dipole fields. The amplitude of pressure is constant at a given distance from a monopole source in free-field conditions. Thus, the directivity pattern can be represented as a circle in a two-dimensional polar plot. The dipole has the same directivity pattern at all radii, as evidenced by the $\cos\theta$ term in Eqs. (6) and (7). This leads to the double-lobed pattern in Fig. 4, with a change of sign of pressure in the field behind the dipole.

The change of pressure amplitude with distance corresponds to simple spherical spreading for the monopole, but the dipole has a near field whose significance varies with frequency. Fig. 5 shows a set of results for a monopole and for dipoles at 6, 12, 24 and 48 Hz, where the sources have the same far-field pressure in the chosen direction. It can be seen how the effect of the near field extends further and further from the source as the frequency is reduced. At 12 Hz, the

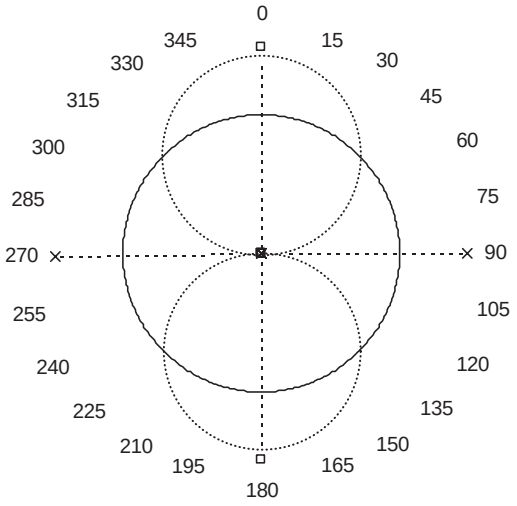

Fig. 4. Directivity patterns for monopole and dipole sources: (———) monopole field; (· · · · · ·) dipole field; (□-----□) dipole axis; (×-----×) normal to dipole axis.

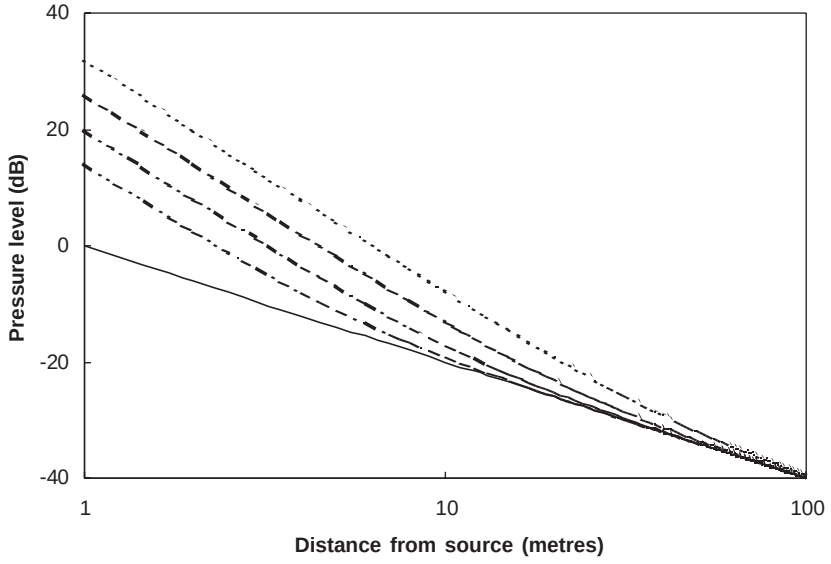

Fig. 5. Pressure change with distance from monopole and dipole sources at different frequencies: (——) monopole; (-----) 6 Hz dipole; (– – –) 12 Hz dipole; (– – –) 24 Hz dipole; (– - – -) 48 Hz dipole.

near-field pressure has the same amplitude as the acoustic pressure at 20 m from the source. At 24 Hz, the corresponding distance is 10 m. These distances are not large in relation to hull dimensions, so the effects of the acoustic field on total hull forces are likely to be significant. Fig. 5 shows also that the near field at 12 and 24 Hz dominates the pressure within a few metres of the source. It is this feature that causes large differences between relative peak pressure and relative total force magnitudes at low multiples of *bpf*.

4.2. Doublets and dipoles

Eqs. (6) and (7) show the equivalence of a fluctuating force applied to the fluid and two monopole sources having opposite signs that are separated by a distance $s \ll \lambda$. It is therefore possible to model the incident pressure field due to a dipole in two ways. First, the explicit field due to a dipole can be included in the BE model. Secondly, the results for monopoles either side of the dipole centre can be subtracted from each other, taking appropriate account of the real (in-phase with the source) and imaginary (out-of-phase with the source) components, and then divided by the separation, to give the result for a doublet of constant strength. This second approach allows results to be derived quickly from those for monopole sources.

The positive monopole is positioned above the negative monopole in the vertical doublet. It is outboard in the transverse doublet and forward in the axial doublet. The positive monopole is used as the phase reference throughout. In common with [5], the out-of-phase hull force component is positive for a phase lag of less than 180° in the following numerical results.

4.3. Force distributions

Cumulative hull forces can be calculated simply by summation of forces on hull elements up to a given station forward of the stern, taking account of the surface orientation and dealing with the in-phase and out-of-phase components separately. They show clearly how the force is distributed along the hull length. This can also be done for port and starboard sides separately, to explore whether the force is dominated by hull excitation on the same side as the assumed propeller source. Results of this type have been presented previously for monopole sources [5]. They are reproduced here in non-dimensional form, to facilitate comparison with new results for dipole sources. The hull forces are easily computed for each of the vertical, transverse and longitudinal directions, but those in the vertical direction tend to be much larger for realistic hull shapes and source positions. Results for all three directions are included in Ref. [5] to illustrate typical behaviour for monopole sources. Attention will be restricted to the vertical direction in the present paper.

5. Convergence of the numerical model

5.1. Comparison with analytic solutions

Results for a complex hull shape can only be derived numerically. Analytical expressions, in the form of Bessel and Hankel function series summations, are available for the submerged sphere

[12]. The first stage of verification of the BE software was to demonstrate that these analytical results could be reproduced accurately, for a range of surface element sizes and wavelengths relative to the diameter of the sphere.

5.2. Independence of precise element distributions

The second stage was to stretch the sphere into an ellipsoidal shape and to introduce a free surface of finite extent. It was shown that the same results could be obtained using different element distributions [6]. Initially, elements were distributed according to surface geometry, so that their density increased towards either end of the ellipsoid. It was then shown that much more rapid convergence can be obtained by increasing the concentration of elements near the source itself to reflect the expected fall in hull pressures with increasing distance from the source [6]. The model of the cruise liner in this paper uses a high density of elements near the stern, which reduces progressively towards the bow. The density of elements describing the sea surface also reduces progressively with distance from the hull.

Convergence of results for the cruise liner model is demonstrated most easily by comparing results for different surface extents and element distributions. Figs. 6 and 7 show cumulative force magnitudes at *bpf* and 4*bpf*, respectively, when a monopole source is positioned at the 40° inboard position shown in Fig. 3. At the lower frequency, results are shown for two sea surface extents with 600 hull elements and for 864 hull elements with the larger surface extent. The number of longitudinal hull segments is increased from 25 to 36 in the latter case, with a corresponding increase in the number of sea surface elements. Results are shown for two sea surface extents at 4*bpf*, differing by a factor of three, and for either 864 or 984 hull elements. The number of

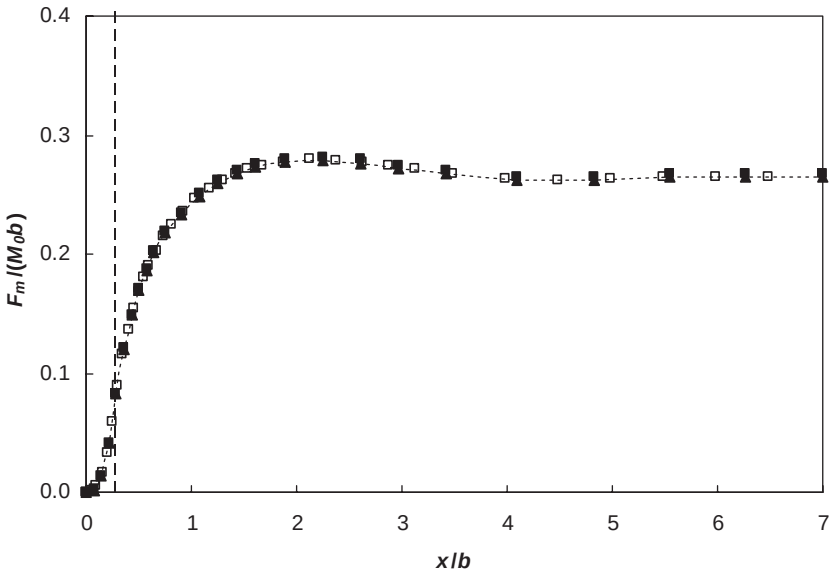

Fig. 6. Cumulative vertical force magnitudes at *bpf*, monopole source at 40° inboard: (- - ▲ - -) $e/b = 9.32$, 600 hull elements; (■) $e/b = 6.21$, 600 hull elements; (□) $e/b = 9.32$, 864 hull elements; (– – –) source position.

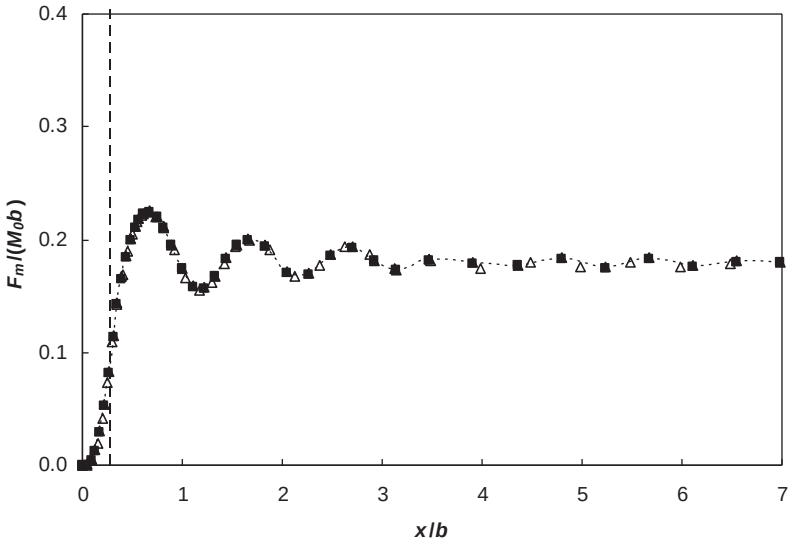

Fig. 7. Cumulative vertical hull force magnitudes at 4*bpf*, monopole source at 40° inboard: (--▲--) $e/b = 3.11$, 984 hull elements; (△) $e/b = 6.21$, 864 hull elements; (■) $e/b = 9.32$, 984 hull elements; (———) source position.

longitudinal hull segments is then either 36 or 41. Results are almost independent of model parameters for frequencies between *bpf* and 4*bpf*, provided that parameters are selected with due regard for λ/b and the complexity of the hull shape.

Dipole sources represent a more severe test of convergence, because results are derived effectively from spatial differentation of results for monopole sources at nearby positions. Fig. 8 shows the effect of changing vertical doublet separation at *bpf*, using $e/b = 9.32$ and 600 hull elements. Cumulative vertical force magnitude distributions are shown for doublet separations with $s/b = 0.012$, 0.12 and 0.18. The latter separation corresponds to the propeller diameter. The results for $s/b = 0.06$ were found to be indistinguishable from those for $s/b = 0.012$. The sensitivity to doublet separation is no larger for other doublet and response directions. Reduction of the doublet separation to very small values can cause divergence, because the differences between monopole fields become too small in relation to their numerical accuracy. A separation $s/b = 0.012$ gives satisfactory convergence at *bpf* and 2*bpf* and is used for subsequent analysis of dipole hull excitation. The separation on the scale of wavelength is then given by $s/\lambda = 0.003$ and 0.006, respectively.

Fig. 9 shows cumulative force distributions computed for a vertical source separation $s/b = 0.012$ at 2*bpf*. This is essentially the result for a vertical dipole. In this case, results for the larger sea surface extent are shown for 600 and 750 hull elements, corresponding to 24 and 30 transverse hull elements with 25 longitudinal elements. There are small differences between results for different sea surface extents, but these are more apparent in the force magnitude than in the shape of the cumulative force distribution. Separate in-phase and out-of-phase forces on port and starboard sides show similar consistency.

The following results have been obtained using element distributions that give convergent results for the specified source parameters. Most are obtained using 600 hull elements with

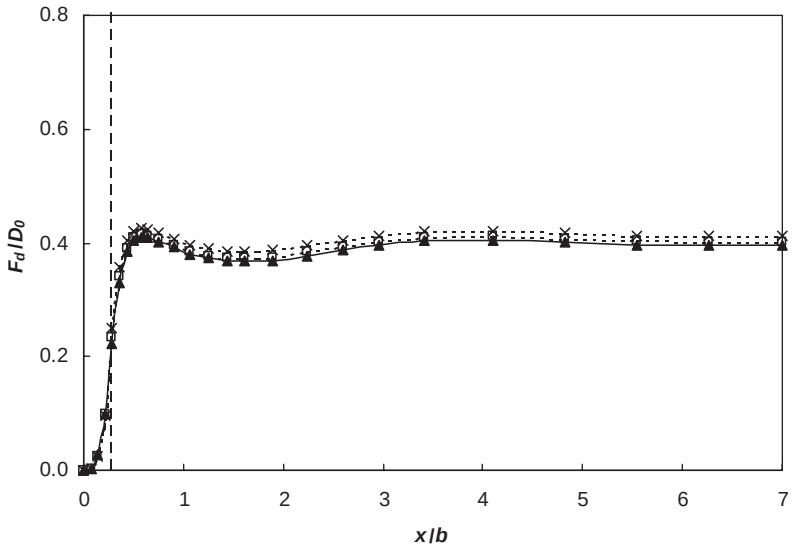

Fig. 8. Cumulative vertical hull force magnitudes at *bpf*, vertical hub doublet: (—▲—) $s/b = 0.01$; (--□--) $s/b = 0.12$; (--×--) $s/b = 0.18$; (———) source position.

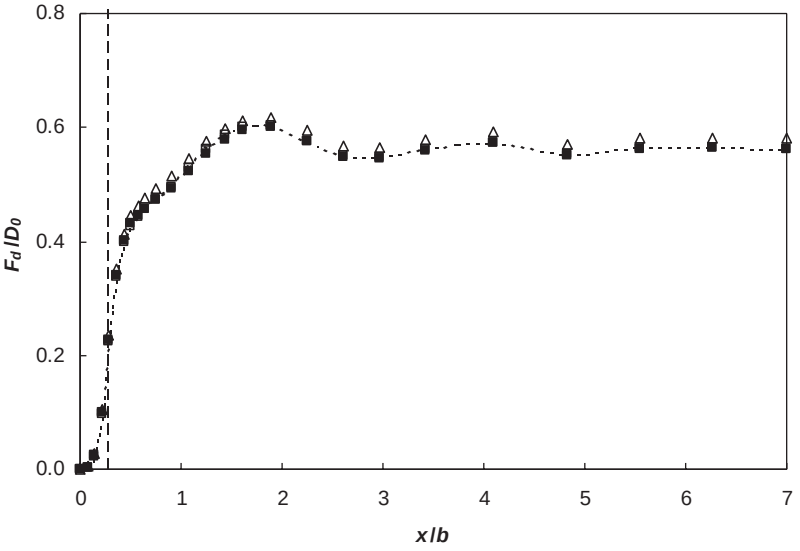

Fig. 9. Cumulative vertical hull force magnitudes at 2*bpf*, vertical hub dipole: (△) $e/b = 9.32$, 750 hull elements; (■) $e/b = 12.42$, 750 hull elements; (--□--) $e/b = 9.32$, 600 hull elements; (———) source position.

$e/b = 9.32$, as shown in Figs. 1–3, at *bpf* and 2*bpf*. Nine hundred and eighty four hull elements are used with $e/b = 3.11$ at 4*bpf*. All results have been checked using different element distributions.

5.3. Confirmation using image methods

An independent acoustic BE model has been developed more recently for efficient analysis of submerged bodies [15], using the same formulation of the Helmholtz equation. The basic procedure for its numerical solution is also included in that paper, together with an indication of the computation times that are presently achievable. Results for floating bodies are derived by replacing the Green function for a monopole or dipole in free space by functions which include the influence of a flat free surface. In effect, this represents an extension of the image techniques developed by Vorus [4] for an incompressible fluid, where the rigid surface of the hull is reflected in the notional flat surface of the sea and where sources below the sea surface are reproduced with opposite sign above the sea surface.

Results using the independent model have been published [15] for a half-submerged ellipsoid having $l/b = 5$ and a circular cross-section, with monopole sources position at representative locations beneath the keel and values of λ/b between 1 and 8. Comparison between submerged and floating bodies has allowed the effects of diffraction and interference to be separated from the powerful effect of the free surface in causing changes with λ/b in the range associated with *bpf* and its low multiples. Cumulative non-dimensional forces on the hull have similar magnitudes and dependence on λ/b to those obtained for the cruise liner hull. In particular, the position of the maximum in the total cumulative force and the oscillatory behaviour in the cumulative force magnitude with increasing distance from the stern show similar dependence on λ/b.

6. Cumulative hull force magnitudes

The magnitudes of cumulative hull forces for increasing x/b are described first for both monopole and dipole sources. This is followed by a discussion of pressure amplitudes on the hull near the propeller for the same sources. The distribution of forces between the port and starboard sides of the hull is then described.

6.1. Monopole sources

Fig. 10 shows how the cumulative force on the hull with respect to x/b changes with frequency for a monopole source at the 40° inboard position in Fig. 3. At *bpf*, the cumulative force reaches a peak value at $x/b \sim 2$, when $\lambda/b = 3.88$. Interference between forces on different parts of the hull then causes it to fall slightly before rising again towards the bow. The cumulative force initially rises more steeply with x/b when frequency is increased to $2bpf$ and $4bpf$, before interference effects become prominent. The peak in the cumulative force therefore moves towards the stern as λ/b is reduced. Oscillation of the cumulative force due to interference effects becomes more prominent with reducing λ/b, primarily because the quenching effect [2] of the free surface is modified [15]. The cumulative force is lower at forward positions, even though hull pressures at forward locations are increased for a given source strength.

The quenching effect of the free surface can be illustrated by moving sources aft from the propeller position. Fig. 11 shows how the total cumulative force on the hull varies as the source is

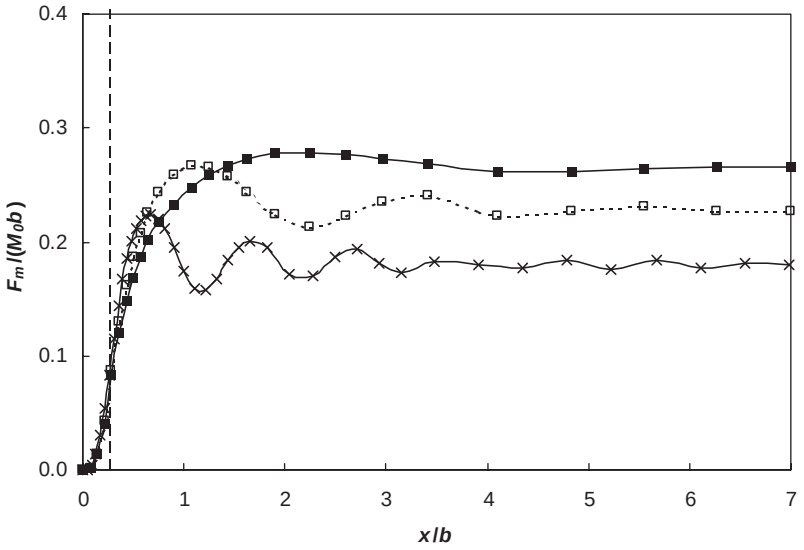

Fig. 10. Cumulative vertical hull force magnitudes, monopole at 40° inboard: (—■—) *bpf*; (--□--) 2*bpf*; (—×—) 4*bpf*; (———) source position.

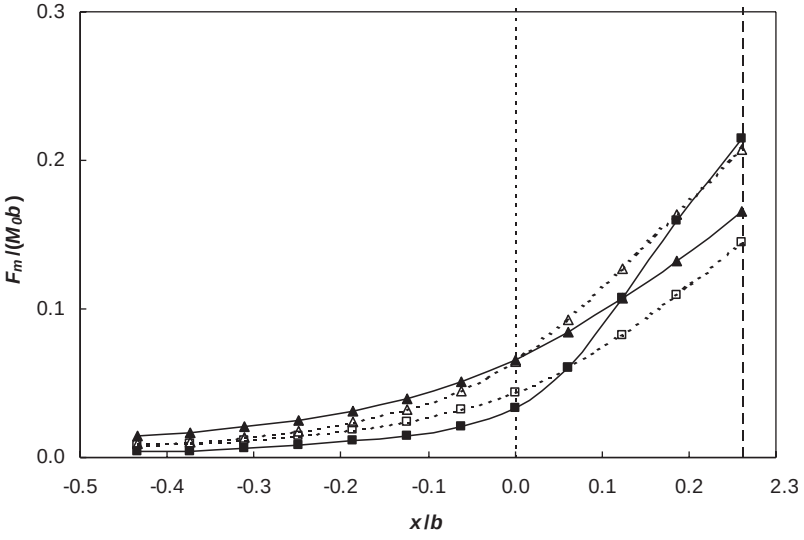

Fig. 11. Total vertical hull forces for different monopole positions at 2*bpf*: (—■—) *tdc*; (—▲—) *bdc*; (--□--) outboard; (--△--) inboard; (-----) stern waterline; (———) propeller position.

moved from the *tdc*, *bdc*, 90° inboard and 90° outboard positions in Fig. 3, at 2*bpf*. The stern waterline and propeller positions are indicated. When the monopole source is aft of the stern waterline, its pressure field approaches that of a vertical dipole at the surface. Thus, the force on the hull is proportional to the source depth when the source is at downstream

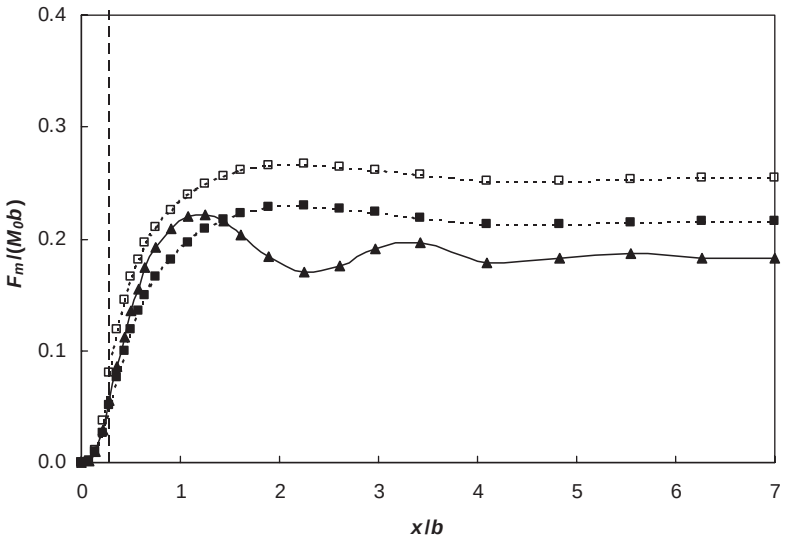

Fig. 12. Cumulative vertical hull force magnitudes, hub monopole at *bpf* and 2*bpf*: (--□--) *tdc* dipole at *bpf*; (--■--) hub dipole at *bpf*; (—▲—) hub dipole at 2*bpf*; (–––) source position.

positions. This is in contrast to sources at the propeller, where the hull force magnitude is highest for the *tdc* position, and lowest for the *bdc* position. Similar behaviour is observed at *bpf* and 4*bpf* [5].

Fig. 12 shows how the cumulative force distribution changes when a monopole source is moved from the hub to the *tdc* position, at *bpf*. It also shows the effect of increasing the source frequency to 2*bpf* when the source is at the hub. The result for the monopole at *tdc* is almost the same as for the source at 90° inboard in Fig. 10, showing the insensitivity of hull forces to source position on the periphery of the propeller disc. Moving the source from *tdc* to the hub causes a change of less than 20% in the total cumulative hull force for a given source strength, even though the hub source is about three times further from the hull. These results provide a benchmark for dipole excitation, where the focus is on sources at the hub and *tdc* positions.

6.2. Dipole sources

Figs. 13–15 show the cumulative vertical force magnitudes on the hull for axial, transverse and vertical dipoles, respectively. The source positions and frequencies are identical to those in Fig. 12 for monopole sources. The effects of source directionality are now clearly apparent.

The axial dipole causes a change in sign of hull pressure at the source location, so that there is a local peak in the cumulative force at the source location $x_s/b = 0.26$. The quenching effect of the free surface is very large when the source is near the stern waterline, so there is only a small contribution to the total force from the region aft of the source, especially for a source at the propeller hub. When the source is near to the hull surface at the *tdc* position, the local peak in the cumulative force at x_s/b is larger. The cumulative force then falls with x/b, before rising again to its maximum well forward of the source location. The directionality and acoustic field of the axial

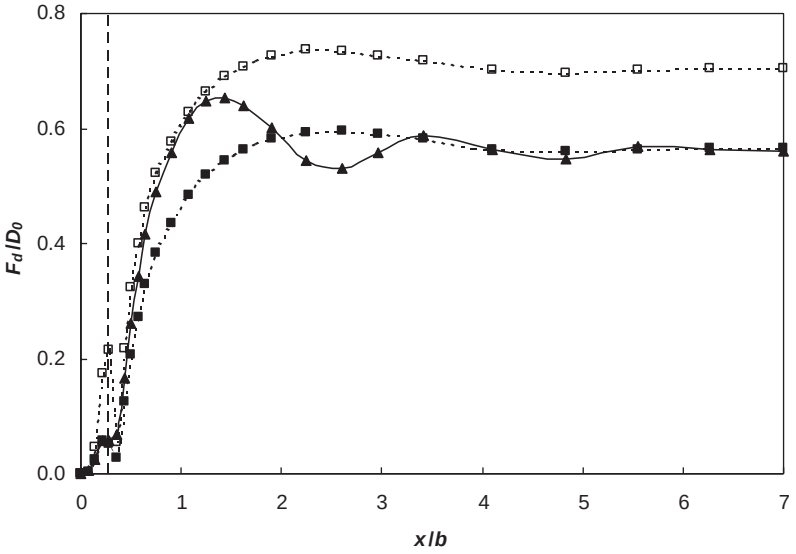

Fig. 13. Cumulative vertical hull force magnitudes, axial dipole at *bpf* and 2*bpf*: (--□--) *tdc* dipole at *bpf*; (--■--) hub dipole at *bpf*; (—▲—) hub dipole at 2*bpf*; (–––) source position.

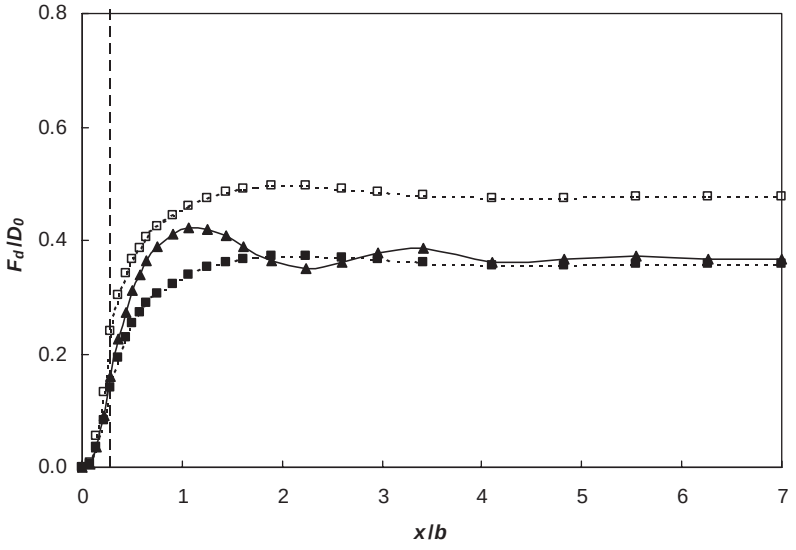

Fig. 14. Cumulative vertical hull force magnitudes, transverse dipole at *bpf* and 2*bpf*: (--□--) *tdc* dipole at *bpf*; (--■--) hub dipole at *bpf*; (—▲—) hub dipole at 2*bpf*; (–––) source position.

dipole are particularly significant, because the near-field pressure is close to zero for hull locations near the source position.

The effect of the near field is also reduced for the transverse dipole and there is partial cancellation between forces inboard and outboard of the source. The cumulative force

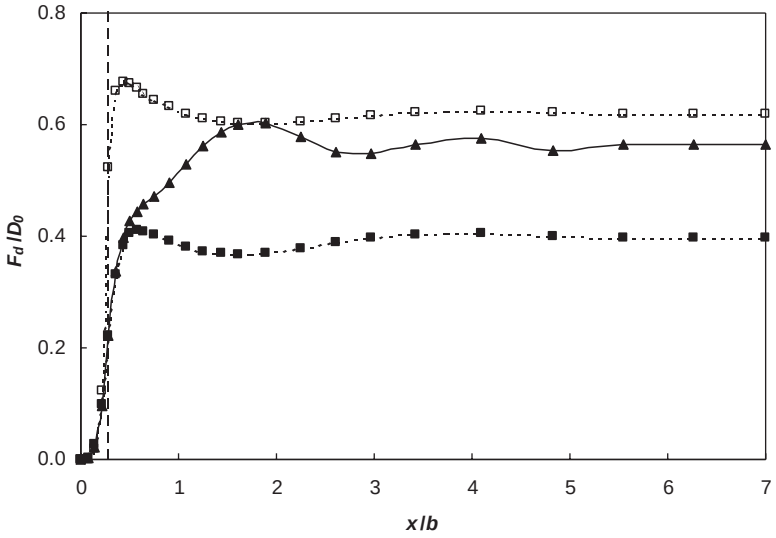

Fig. 15. Cumulative vertical hull force magnitudes, vertical dipole at *bpf* and 2*bpf*: (--□--) *tdc* dipole at *bpf*; (--■--) hub dipole at *bpf*; (—▲—) hub dipole at 2*bpf*; ––– source position.

distributions show strong similarities to those for a monopole. Moving the axial or transverse dipole from the hub to the *tdc* location changes the maximum in the cumulative vertical hull force by less than 25%, only slightly more than for the monopole source. Changes in the total cumulative forces, obtained by integration over the whole of the hull surface, are of similar order to changes in the peak cumulative forces, but are not identical.

The results for the vertical dipole show the powerful effect of its near field, whose maximum is directed toward the hull surface above the source. The maximum in the cumulative force is now reached at $x/b \sim 0.6$ when the source is at the hub. It is even nearer the stern when it is moved to the *tdc* position. Also, the maximum in the cumulative force distribution with respect to x/b increases by more than 60% with the change in source position at *bpf*, over twice the increase for either the monopole or the axial and transverse dipoles. The most striking change for the vertical dipole occurs between results at *bpf* and 2*bpf*. The cumulative force is almost the same for $x/b < 0.5$ at *bpf* and 2*bpf*, where the near field is dominant, but then continues to rises sharply with increasing x/b at 2*bpf*.

It is only in the region $x/b < 0.5$, either side of the source position at $x_s/b = 0.26$ where near-field effects are dominant, that similar behaviour is observed at *bpf* and 2*bpf* both for the monopole and for dipoles in different directions. This is a potentially important result, because it shows that the inability to scale λ/b in model-scale experiments is of reduced importance, so far as hull pressures near the source are concerned. Indeed, similar results in this small region can be obtained using the Helmholtz equation for $\lambda/b > \sim 2$ and Laplace's equation for infinite λ/b. This allows the prospect of estimating total hull forces by using measurements of pressure amplitude and phase near the propeller to define equivalent acoustic source strengths.

For each dipole direction, the total vertical force on the hull is a significant proportion of the dipole force. The force ratio F_d/D_0 lies in the range from 0.37 to 0.70 for all the specified dipole

locations and directions at *bpf* and 2*bpf*. In the case of the axial dipole, the range is 0.56–0.70. These results echo an important analysis by Chertock [16], who showed that the ratio of the force on the outside of a submarine hull to the force transmitted by the tailshaft is almost constant, regardless of hull shape and the precise propeller force distribution. Chertock's analysis did not include the effects of a finite speed of sound, nor was there any need to represent the remote sea surface. The ratio of the hull force to the dipole force is much larger for a cruise liner than a submarine, because the propeller is under, rather than behind, the hull. Also, the results for a surface ship are influenced significantly by the longitudinal location of the propeller relative to the stern waterline.

7. Hull pressure distributions

The in-phase and out-of-phase components of hull pressure, averaged over the area of each hull BE, are direct outputs from the numerical model. The pressure amplitude can then be represented as a solid boundary factor (SBF), if desired [5,15]. This represents the ratio of the pressure amplitude at a given location on the rigid hull surface, in the presence of the sea surface, to its value at the same location in free-field conditions for an identical source. Although the values of SBF are usually less than about 3 for monopole sources, for any location on the hull, much larger values can arise with dipole sources. This is because the free-field pressure is zero normal to the dipole axis, so that weak diffraction can lead to locally infinite SBF in a fully resolved model. For this reason, distributions of pressure amplitude near to the source are shown directly for different dipole orientations.

A striking feature of the results for monopole and dipole sources shown in Figs. 12–16 is that the vertical hull forces are of similar magnitude if $M_0 b \sim 2D_0$ at *bpf* and 2*bpf*, for any dipole orientation. The non-dimensional hull pressures for comparable vertical hull forces due to dipole and monopole sources are therefore $p_d b^2/D_0$ and $2p_m b/M_0$. This modified scaling will be used here for comparison of hull pressure distributions due to monopole and dipole sources. Thus, the non-dimensional pressure due to the monopole has been doubled, so that the comparison is for similar hull forces.

Fig. 16 shows the non-dimensional hull pressure at $x/b = 0.25$, for each orientation of a dipole at the propeller hub and also a monopole source at the same location, at *bpf*. This section is only slightly aft of the propeller disc at $x_s/b = 0.26$, so it represents pressures above the propeller. Fig. 17 shows the corresponding pressure distributions at $x/b = 0.31$, slightly forward of the propeller disc.

It is immediately apparent that the pressure distributions due to dipole sources change dramatically with dipole orientation and also differ markedly from those for a monopole. This is a consequence of the dipole directivity and near-field characteristics shown in Figs. 4 and 5. The axial dipole gives low pressures above the propeller, which increase initially in either the forward or aft direction, before falling again at larger distances. The transverse dipole also gives low pressure above the source, which increases with transverse displacement. The vertical dipole has a powerful near field in the vertical direction, so there is a sharp peak in pressure above the propeller hub. The monopole pressure is relatively low, but changes much less rapidly with distance in the immediate vicinity of the source.

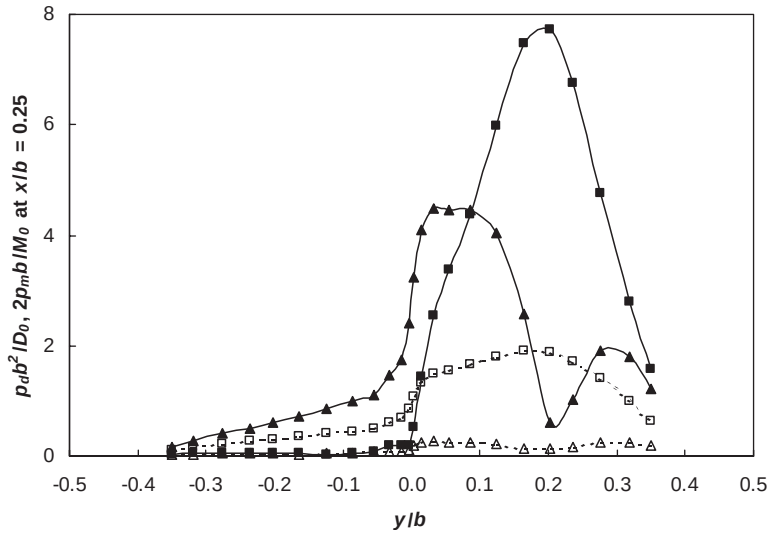

Fig. 16. Hull pressure at $x/b = 0.25$ for *bpf* sources at propeller hub: (—■—) vertical dipole; (—▲—) transverse dipole; (--△--) axial dipole; (--□--) monopole.

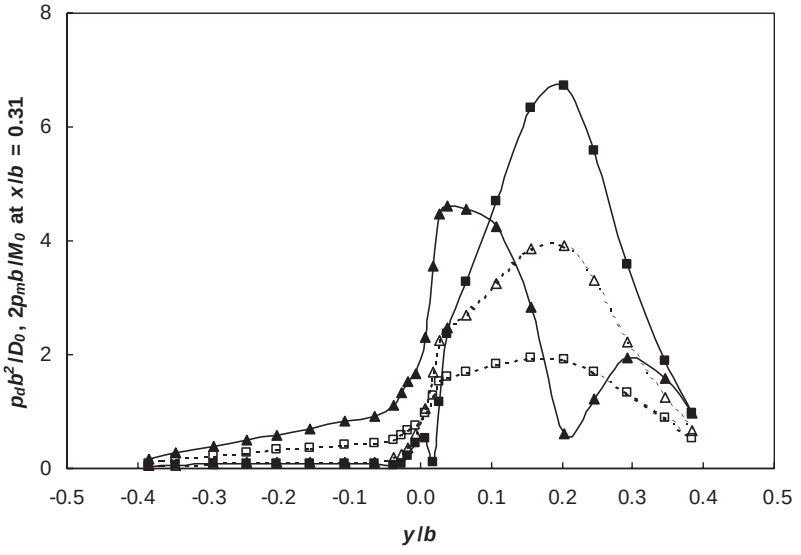

Fig. 17. Hull pressure at $x/b = 0.31$ for *bpf* sources at propeller hub: (—■—) vertical dipole; (—▲—) transverse dipole; (--△--) axial dipole; (--□--) monopole.

Fig. 18 shows the pressure distributions at $x/b = 0.25$, at $2bpf$. The distributions are similar to those shown for hub sources in Fig. 16 at *bpf*. The same is true of other locations near the propeller. This similarity of pressure distributions on the hull near the propeller for different values of λ/b corresponding to low multiples of *bpf* has significant implications for the derivation of hull disturbing forces from model-scale tests.

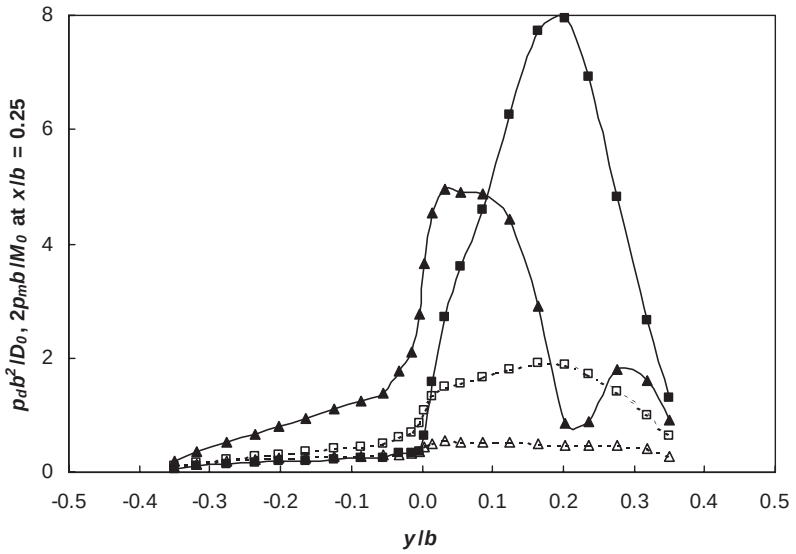

Fig. 18. Hull pressure at $x/b = 0.25$ for $2bpf$ sources at propeller hub: (—■—) vertical dipole; (—▲—) transverse dipole; (--△--) axial dipole; (--□--) monopole.

Near-field effects increase considerably when the source is moved closer to the hull. This is shown in Figs. 19 and 20 at *bpf*, where the sources are now at the *tdc* position on the starboard propeller disc, as shown in Fig. 3. The vertical scale is the same in these two figures, but has been increased by a factor of 10 relative to Figs. 16 and 17. The peak in the pressure due to the vertical dipole has not been fully resolved, but it dominates other features. It has increased by a factor of more than 7, where the total vertical force has changed by a factor of 1.6. The pressures due to axial and transverse dipoles have also increased much more than the pressure due to the monopole source. Large changes in local pressures with source location in the propeller plane are in sharp contrast to the much smaller changes in hull disturbing forces. It is this feature that makes it so important to exercise care in relating hull pressures to hull forces. It also shows why design for low hull pressures near the propeller, which tends to demand large clearances between propeller sources and the hull surface, is not necessarily the same as design for low vibration excitation, which demands low source strengths.

The effect of using artificial boundary conditions in place of the free surface of the sea has not been explored explicitly in this paper, but BE analysis can be used to examine the effects of water tunnel boundaries, for example. High fidelity in modelling propeller load distributions and cavitation, using relatively high Reynolds numbers, might then be extended to the prediction of hull force distributions at full scale.

8. Forces on port and starboard sides of the hull

It is common in model-scale experiments, as well as in numerical simulations, to assume that only forces on the same side of the hull as the propeller source are significant. In order to explore

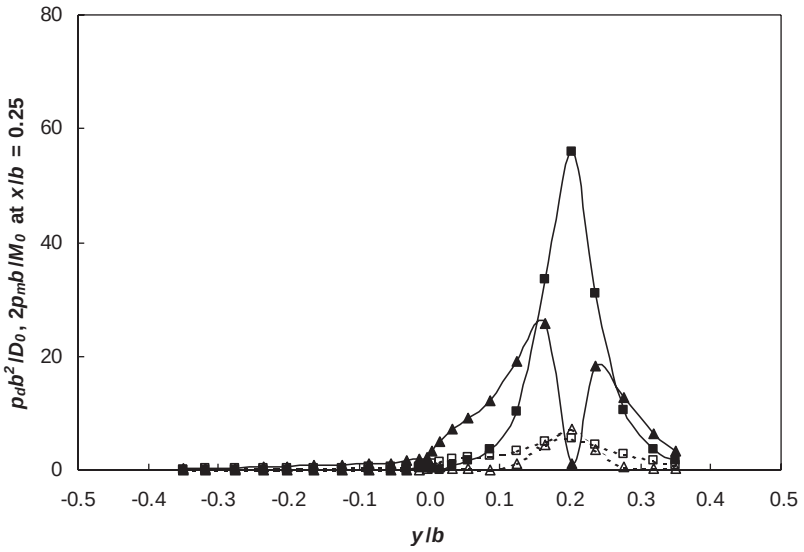

Fig. 19. Hull pressure at $x/b = 0.25$ for *bpf* sources at propeller *tdc*: (—■—) vertical dipole; (—▲—) transverse dipole; (--△--) axial dipole; (--□--) monopole.

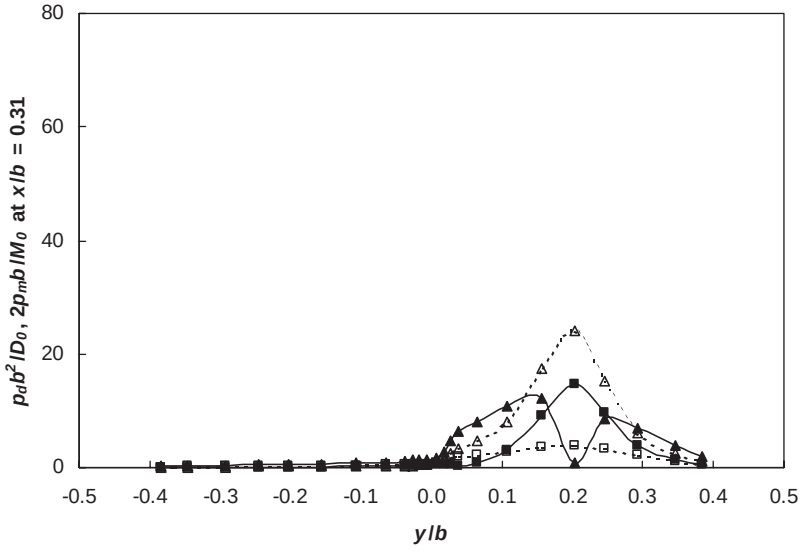

Fig. 20. Hull pressure at $x/b = 0.31$ for *bpf* sources at propeller *tdc*: (—■—) vertical dipole; (—▲—) transverse dipole; (--△--) axial dipole; (--□--) monopole.

whether this is realistic, the in-phase and out-of-phase cumulative vertical forces have been computed separately for the port and starboard sides. The results presented here are primarily at *bpf*.

8.1. Monopole sources

Fig. 21 shows the cumulative force distributions for a monopole source at the 40° inboard position on the propeller periphery, at *bpf*. Similar results can be obtained for any monopole location on the upper part of the propeller periphery, confirming the insensitivity of hull forces to the precise location of a source having constant strength. The in-phase force on the port side is small relative to the force on the starboard side, but not negligible. The out-of-phase forces are, however almost identical. This reflects the behaviour of the e^{-ikr}/r term in Eq. (3), whose imaginary part is almost invariant with r when kr is small. When x/b is large, the distance from the source to mirrored points on the port and starboard sides of the hull is almost the same.

Fig. 22 shows the effect of moving the monopole source to the propeller hub. The in-phase forces are smaller on both sides of the hull, but the out-of-phase forces are hardly changed from the location on the propeller periphery. The contribution to the hull force from the immediate vicinity of the propeller on the starboard side has changed more than other contributions. This result for the hub monopole can now be compared with those for hub dipoles in different directions.

8.2. Dipole sources

Figs. 23–25 show results for the axial, transverse and vertical dipoles, respectively, at *bpf*. The reversal of sign near the propeller location for the axial dipole is particularly clear for the in-phase force on the starboard side in Fig. 23. The ratio of the in-phase forces on the starboard and port sides is greater than for the monopole, because of the dipole field directivity. The out-of-phase

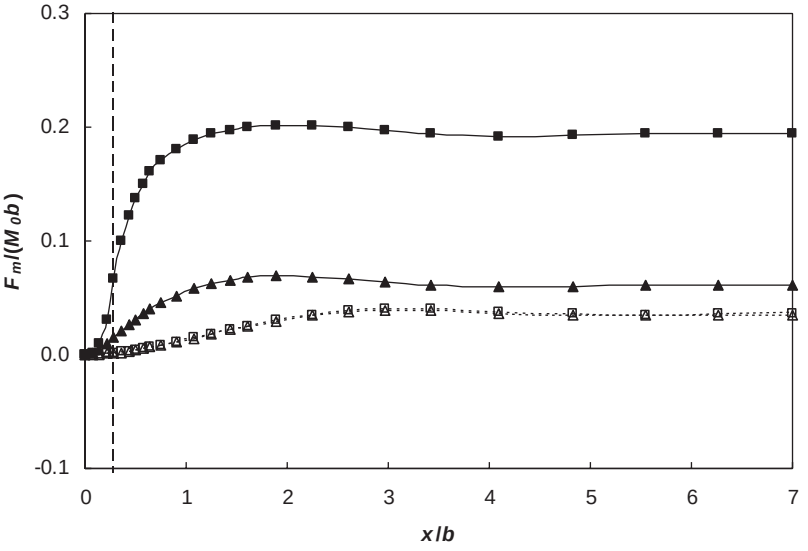

Fig. 21. Cumulative vertical hull forces, port and starboard, *bpf* monopole at 40° inboard: (—▲—) port, in-phase; (--△--) port, out-of-phase; (—■—) starboard, in-phase; (--□--) starboard, out-of-phase; (– – –) source position.

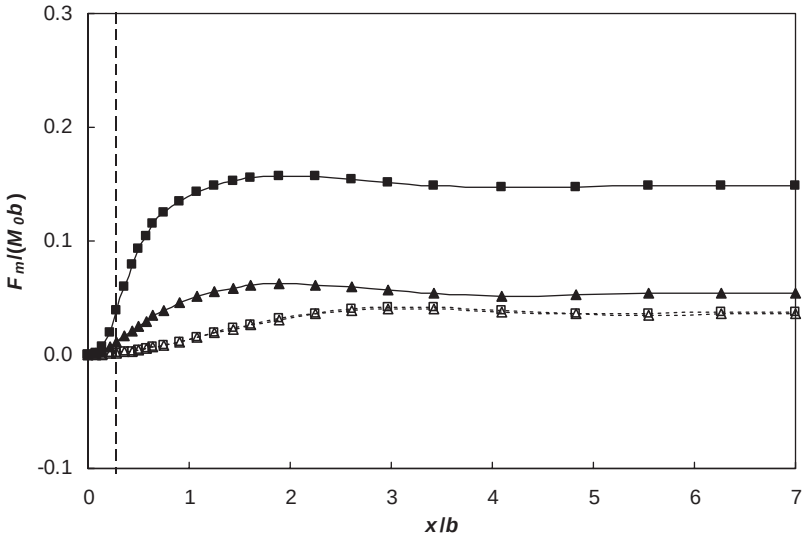

Fig. 22. Cumulative vertical hull forces, port and starboard, *bpf* hub monopole: (—▲—) port, in-phase; (--△--) port, out-of-phase; (—■—) starboard, in-phase; (--□--) starboard, out-of-phase; (–––) source position.

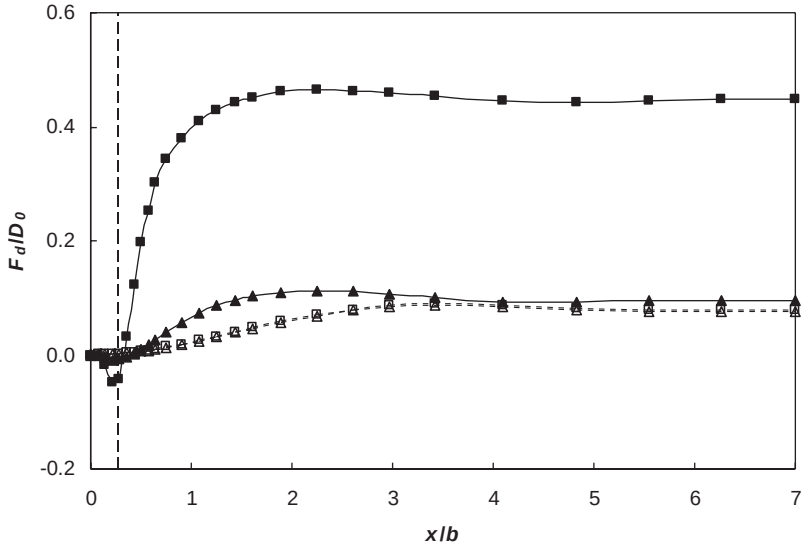

Fig. 23. Cumulative vertical hull forces, port and starboard, *bpf* axial hub dipole: (—▲—) port, in-phase; (--△--) port, out-of-phase; (—■—) starboard, in-phase; (--□--) starboard, out-of-phase; (–––) source position.

components are almost identical on the port and starboard sides, as for the monopole source at the same location.

The in-phase forces due to the transverse dipole shown in Fig. 24 have almost equal magnitude on each side of the hull, primarily as a result of its directivity pattern and partial cancellation of

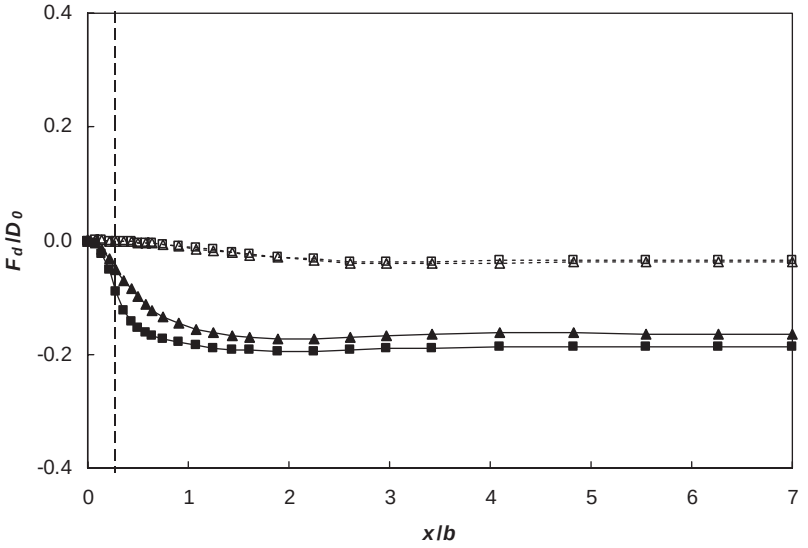

Fig. 24. Cumulative vertical hull forces, port and starboard, *bpf* transverse hub dipole: (—▲—) port, in-phase; (--△--) port, out-of-phase; (—■—) starboard, in-phase; (--□--) starboard, out-of-phase; (———) source position.

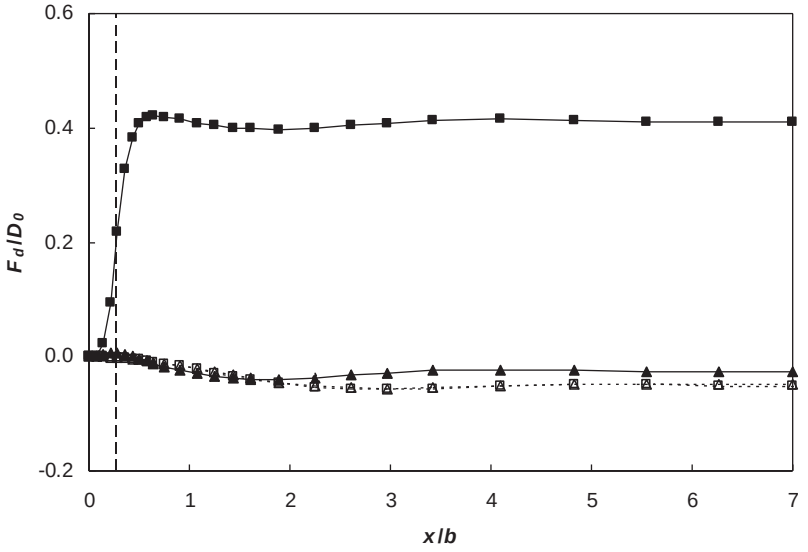

Fig. 25. Cumulative vertical hull forces, port and starboard, *bpf* vertical hub dipole: (—▲—) port, in-phase; (--△--) port, out-of-phase; (—■—) starboard, in-phase; (--□--) starboard, out-of-phase; (———) source position.

forces on the starboard side of the hull. The in-phase forces are now opposite to the dipole direction. Fig. 25 shows that the vertical force due to the vertical dipole is concentrated on the same starboard side as the source. In both cases, the out-of phase forces are almost identical on the port and starboard sides.

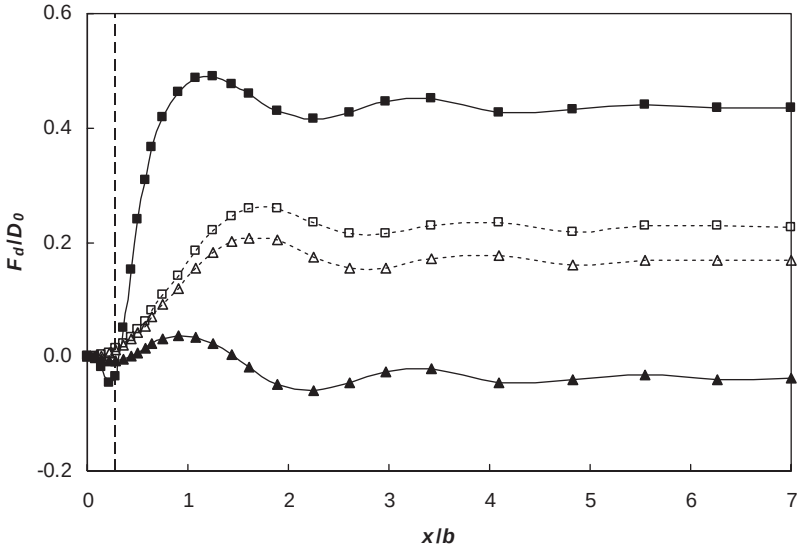

Fig. 26. Cumulative vertical hull forces, port and starboard, 2*bpf* axial hub dipole: (—▲—) port, in-phase; (--△--) port, out-of-phase; (—■—) starboard, in-phase; (--□--) starboard, out-of-phase; (———) source position.

When the frequency is increased, the out-of-phase forces have increased magnitude relative to the in-phase forces, and also become significantly different on port and starboard sides. This is illustrated for the axial dipole in Fig. 26, at 2*bpf*.

9. Conclusions

An acoustic BE model of a modern twin-screw cruise liner hull has been used to compute the hull pressure distributions and cumulative forces due to monopole sources and dipole sources in different directions at the propeller location. The Helmholtz equation, rather than the Laplace equation, is solved to allow inclusion of the effects of a finite speed of sound underwater, in the presence of the sea surface and a hull boundary that is assumed to be rigid. The model itself can accommodate stationary and moving sources of arbitrary complexity, but stationary sources are used to explore underlying results. Dipole sources are used to represent the net effects of fluctuating forces at the propeller, while monopole sources represent the principal effects of cavitation.

A real propeller will have pressure fields that are due to a spatial distribution of monopole and higher order sources, above cavitation inception. Some of the higher order sources are associated with the effects of fluid flow and the spatial distribution of fluctuating cavities due to cavitation. They will disappear when cavitation is suppressed. Others are associated with fluctuating and rotating forces on blades having finite thickness. This analysis of hull excitation due to monopole and dipole sources has illustrated some of the underlying features that are present in the hull force distributions and which should influence interpretation of data from model and full-scale experiments.

The BE model was verified initially by comparing numerical and analytical results for a submerged sphere, with a progressive transition through floating ellipsoids to the complex shape of the floating cruise liner hull. Convergence has been demonstrated for the cruise liner hull model by showing that the same results can be obtained using different sea surface extents and element distributions, for various ratios of underwater sound wavelength relative to hull dimensions.

The cruise liner chosen for analysis has a maximum propeller *bpf* of 12 Hz, while the waterline length, beam and draught are 251, 32.2 and 8.3 m, respectively. The 5.8 m diameter propellers are 8.4 m forward of the stern waterline and have a hub depth of 5.4 m. They are separated by 13.0 m in the transverse direction. These dimensions are typical of large, modern, twin-screw cruise liners. The underwater sound wavelength λ at *bpf* is slightly less than four times the beam, if the sound speed is assumed to be 1500 m/s.

Results have been presented in non-dimensional form by using the hull beam b as a reference length scale. The analysis is primarily at non-dimensional wavelengths corresponding to *bpf* and 2*bpf*, in order to demonstrate how the fluctuating pressures and forces are influenced by wavelength and source type. The excitation has been specified as sinusoidal at each frequency, but the results are also specimen transfer functions relating the spectral characteristics of the source to the consequent hull excitation.

9.1. Hull forces and pressure distributions for different sources

It has been shown for the typical cruise liner hull how the relationships between hull pressure fluctuations, forces computed by integration over a small area above the propeller, and total hull forces, vary according to the nature and location of the acoustic source that causes them. A monopole of strength M_0 kg/s^2 and a dipole of strength D_0 N with any orientation at the same location, lead to similar total hull forces if $M_0 b/D_0 \sim 2$ at *bpf* and 2*bpf*. Much larger ratios of $M_0 b/D_0$ are found in practice for propellers with localized cavitation in a twin-screw ship at high propulsive power. Nevertheless, these larger ratios may still be insufficient to ensure that hull pressures near to the propeller are dominated by the sources which govern hull vibration excitation.

The total vertical hull force increases by less than 25%, 35% and 55% for axial, transverse and vertical dipoles, when the source is moved from the hub to the top of the cruise liner propeller, where it is three times closer to the hull surface. The change is less than 20% for a monopole source. The fluctuating pressure on the hull above the source shows changes that are an order of magnitude greater than the changes in total hull forces. Thus, the net hull excitation is relatively insensitive to source position, while maximum hull pressures are not. It is these properties that necessitate careful interpretation of fluctuating pressures in the vicinity of the propeller, if the net hull excitation that causes vibration is to be estimated accurately.

A compact monopole with strength M_0 at the propeller hub, 3.3% of the hull length forward of the stern waterline, leads to a total vertical hull force of about 0.22 $M_0 b$ at *bpf*. The force over the aft-most 5% of the hull length is about half this value. A fluctuating thrust at the propeller hub of D_0 at *bpf* leads to a total vertical force on the hull of $0.57 D_0$, but a force that is only $0.20 D_0$ over the aft-most 5% of the hull length. In the case of the axial dipole, the range of integration has a critical effect, because the cumulative force is near to zero when integration is to just forward of the propeller.

A fluctuating transverse hub force of D_0 at *bpf* leads to a total vertical force of $0.36D_0$, but the cumulative force over the aft-most 5% of the hull length is $0.25D_0$. In that case, the hull force is distributed almost equally between port and starboard sides of the hull. On the other hand, a vertical fluctuating force of D_0 at the hub leads to a total vertical hull force of about $0.40D_0$ and a cumulative force that is also $0.40D_0$ over the aft-most 5% of the hull length. Furthermore, this force is concentrated on the same side as the propeller source. These differences reflect the directivity and near-field properties of the dipole.

9.2. Improved interpretation of results from model-scale tests

Widely used physical or numerical modelling techniques for hull force estimation do not take account of the finite speed of sound underwater. Strictly, the sound wavelength λ at a given scaled frequency should have the same ratio to hull dimensions at model and full scale, if the pressure field over the hull surface is to be reproduced correctly. At model scale $1/s$, λ/b is a factor of $\sqrt{s}$ too large when Froude number is scaled correctly, if the speed of sound underwater is the same at full scale and in model-scale tests. Thus, integration of pressure over the whole of the hull surface will not represent full-scale hull excitation accurately, even if the fluctuating propeller forces and cavitation regions are reproduced perfectly. There is, however, a possible extrapolation approach for towing tank experiments, because pressures in the immediate vicinity of the propeller are influenced only slightly by the finite speed of sound, if the water surface is positioned correctly. If the acoustic sources can be derived correctly from the model experiments, then an acoustic BE model can be used to determine the hull forces.

A rather different approach is required for prediction of hull forces from pressure fluctuation measurements in a water tunnel, where there is no free surface. The pressure distribution will be influenced by tunnel boundaries, to an extent that is usually not known precisely. Only pressures in the immediate vicinity of the propeller are likely to be unaffected by these unwanted boundaries, even if the full-scale propeller source characteristics can be reproduced perfectly. Again, there is the prospect of improved hull force estimation using BE models, because the effects of tunnel boundaries can also be estimated using the numerical model.

9.3. The need for improved definition of ship requirements

The analysis has shown why specification of maximum hull pressure fluctuations at, say, *bpf* can lead to selection of a propeller design that is sub-optimal in terms of vibration excitation. Increased tip clearance and reduced propeller diameter, for example, will often lead to reductions in maximum hull pressure. Such an approach can, however, have an adverse effect on total hull disturbing forces if the net source strength increases as a result, apart from effects associated with changes in *bpf* at a given propulsive power. Lower vibration might be achievable in such cases by using a larger, reduced speed propeller with smaller clearances and increased hull pressures above the propeller. This is because maximum hull pressure is determined by the near field of the propeller, while the overall hull excitation is governed more by the far field, which also determines underwater radiated noise. A change of emphasis from maximum hull pressure fluctuations to maximum acoustic source strengths would facilitate optimal design in these circumstances.

Acoustic BE models, combined with finite element models that allow hull dynamic characteristics to be represented, offer improved prospects for linking vibration requirements directly to hull excitation and therefore to propeller source characteristics. In particular, acceptable hull excitation can be related to dipole and monopole source strengths at different locations and frequencies. At the same time, there is a clearer link between underwater radiated noise and hull vibration excitation at low frequencies.

Acknowledgements

Christina Bloor is grateful to the EPSRC and to BAE SYSTEMS for their joint funding of her CASE studentship in the Department of Applied Mathematics and Theoretical Physics at Cambridge. The authors greatly appreciate encouragement by her academic supervisors, the late Professor David Crighton, FRS and Dr Nigel Peake, and by P&O Princess Cruises. They are also grateful to Meyer Werft in Papenburg for permission to use real hull data in the numerical model and to Dr Iain Thompson of BAE SYSTEMS for his help in creating robust computer programs from research variants.

References

[1] C. Johanssen, Recent considerations on dealing with propeller induced hull pressure pulses, *Proceedings of NAV2000*, Venice, 19–22 September 2000.
[2] J.P. Breslin, P. Andersen, *Hydrodynamics of Ship Propellers*, Cambridge University Press, Cambridge, 1994.
[3] J.-K. Choi, S.A. Kinnas, Numerical model of cavitating propeller inside of a tunnel, *Journal of Fluids Engineering* 121 (1999) 297–304.
[4] W.S. Vorus, A method for analysing the propeller-induced vibratory forces acting on the surface of a ship stern, *Transactions SNAME* 82 (1974) 186–210.
[5] R. Kinns, C.D. Bloor, Fluctuating hull forces due to propeller cavitation, *Transactions of the Royal Institution of Naval Architects Part A* 144 (2002) 41–70.
[6] C.D. Bloor, A Study of the Acoustic Pressures on a Ship's Hull due to its Propellers, PhD Thesis, Cambridge University, 2002.
[7] J.S. Jensen, A.R. Sørensen, U.M. Rasmussen, Recent experience in cavitation performance and structural vibrations for fast ferries, *Proceedings of the Second International EuroConference on High Performance Marine Vehicles*, HIPER'01, Hamburg, 2–5 May 2001.
[8] M.J. Lighthill, *Waves in Fluids*, Cambridge University Press, Cambridge, 1978.
[9] G. Kirchhoff, Zur Theorie der Lichtstralen, *Annalen der Physik und Chemie* 18 (1883) 663–695.
[10] B.B. Baker, E.T. Copson, *The Mathematical Theory of Huygen's Principle*, Oxford University Press, Oxford, 1939.
[11] R.P. Shaw, Boundary integral equation methods applied to wave problems, in: P.K. Banerjee, R. Butterfield (Eds.), *Developments in Boundary Element methods—1*, Applied Science, Barking, 1979.
[12] E.A. Skelton, J.H. James, *Theoretical Acoustics of Underwater Structures*, Imperial College Press, London, 1997.
[13] R. Kinns, C.D. Bloor, The effect of shaft rotation direction on cavitation-induced vibration in twin-screw ships, *Proceedings of NCT'50*, Newcastle, 3–5 April 2000.
[14] D. Ross, *Mechanics of Underwater Noise*, Peninsula Publishing, Los Altos, CA, 1987.
[15] R. Kinns, N. Peake, O. Rath Spivack, Hull vibration excitation by propeller sources: a link between hydrodynamics and marine acoustics, *Proceedings of the 24th Symposium on Naval Hydrodynamics*, Fukuoka, Japan, 8–13 July 2002.
[16] G. Chertock, Forces on a submarine hull induced by the propeller, *Journal of Ship Research* 9 (1965) 122–130.